16th Australasian Wind Engineering Society Workshop
Brisbane, Australia
18-19 July, 2013

DNS of Escarpment Flow for Wind Turbine Siting

D. F. Xie, H. M. Blackburn and J. Sheridan

Department of Mechanical & Aerospace Engineering
Monash University, Victoria 3800, Australia

Abstract

Turbulent flows over a forward-facing ramp (FFR) were investigated using numerical methods. The present direct numerical simulations (DNS) were conducted under conditions with approaching wind directions from 0° to 45° with 15° difference in order to examine flow features and the effect of inflow yaw angle. A spatially developed turbulent inflow was generated by applying a *recycled boundary condition*. Reynolds number is 2000, based on ramp height and bulk streamwise velocity of the oncoming flow, and the ramp is assumed to be infinitely extended in the spanwise direction. DNS results show quantitative turbulent statistics and structures of boundary layers over a FFR.

Introduction

Site selection of wind turbines is a very important decision in the development of an onshore wind farm, as it affects both power production and fatigue life. With a continuing expansion of wind energy demand, sites with complex terrain have become more favorable candidates due to localized wind speed-up, which may introduce significant dynamic loading as well as increased energy availability. However the wind field at sites with complex topography is more difficult to predict because the flow is highly turbulent as a result of separation and reattachment.

Despite significant efforts made in the past to understand flow over a complex terrain, such as the forward-facing step (FFS) (Sherry et al., 2010), escarpment (Jensen, 1983; Bowen and Lindley, 1977) and the cliff with sawtooth (Cochard et al., 2012), few investigations have dealt with a yawed flow. There are two main reasons for this: first, until very recently, the nature of separated turbulent flow has been poorly understood; second, wind tunnel tests have failed to accurately predict the speed-up ratios in yawed flows due to the influence of end effects. It is believed that flow features, such as speed-up and separation, are highly influenced by the approaching wind direction. However the mechanics and physics behind such flow is poorly understood. Therefore, this research proposed an investigation of turbulent flow over a two-dimensional escarpment using numerical methods. The motivation of this paper was to access a better understanding of flow features by topographical effect. An equally important aspect was to investigate yaw effects on turbulence structure downstream.

Methods

The yawed flow over an escarpment, as sketched in Figure 1, is used to investigate the sweep-dependence under this configuration for moderate yaw angles, i.e. $\alpha \leqslant 45°$. A considerable cross flow develops over time, resulting in a skewed mean velocity profile. The distance of reattachment location is presented by R_x, which is measured in the direction normal to the ramp edge. $R_{\widehat{x}}$ represents the reattachment point along the direction of incoming flow.

The governing equations used in the DNS are the incompressible Navier–Stokesequation without buoyancy terms, as

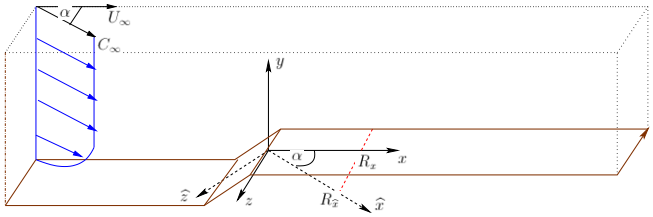

Figure 1: Ramp normal coordinates x, y, z and coordinates $\widehat{x}, \widehat{y}, \widehat{x}$ aligned with the incoming flow.

follows:

$$\nabla \cdot \mathbf{u}^* = 0, \frac{\partial \mathbf{u}^*}{\partial t^*} + (\mathbf{u}^* \cdot \nabla)\mathbf{u}^* = -\frac{1}{\rho}\nabla p^* + \nu \nabla^2 \mathbf{u}^* + \mathbf{f}, \quad (1)$$

where $\mathbf{u}^* = [u, v, w]^T$ is the velocity vector, ρ is density, p^* is pressure, ν is kinematic viscosity and $\mathbf{f}$ is body force per unit mass of the flow. $\mathbf{f}$ is introduced so that flow rate will be constant or oscillate around the defined level. By prescribing a spanwise $\mathbf{f}$ we could introduce a spanwise flow rate, thus achieve a yawed inflow.

With the non-dimensional case, new variables are achieved using the free-stream velocity U_∞ and escarpment height H:

$$\frac{\partial \mathbf{u}}{\partial t} + (\mathbf{u}.\nabla)\mathbf{u} = -\nabla p + \frac{1}{Re_H}\nabla^2 \mathbf{u} + \mathbf{f}, \quad (2)$$

where Re_H=$U_\infty H/\nu$ is the Reynolds number, $p = p^*/\rho {U_\infty}^2$ is static pressure. The present DNS based on the spectral element method is carried out under conditions of constant Reynolds numbers based on the free stream component normal to the ramp, U_∞ and the height of the ramp, H. The ramp height is fundamentally set to $1/5$ of the boundary layer thickness. Note that the Reynolds number based on the boundary layer thickness is used in the calculation, but the Reynolds number based on the step height is employed in the result, because the appropriate Reynolds number which may represent a FFR flow is Re_H. The detailed computational conditions are indicated in Table 1, which includes the Reynolds numbers and domain information.

Re_τ	10000
Re_H	2000
ramp slope	45°
domain size ($x \times y \times z$)	$40H \times 5H \times 2\pi H$
yaw angles(α)	0°, 15°, 30°, 45°

Table 1: Computational conditions.

Figure 2 presents the two-dimensional outline of the element mesh and the close-up on the area near the ramp along with a schematic of the recycled boundary condition. Non-uniform grids around the ramp are arranged in streamwise and wall-normal directions so as to adequately capture turbulent motions.

The boundary conditions for the velocity field are the non-slip conditions on the walls, and free stream on the upper boundary. A special kind of boundary condition is prescribed at the inlet to the domain to generate a spatially developed turbulent inflow without the need for a separate development section. It is a variation of the method for generation of turbulent inflows proposed by Lund et al. (1998), here is referred to as *recycled boundary condition*. Periodic boundary is used in the spanwise direction.

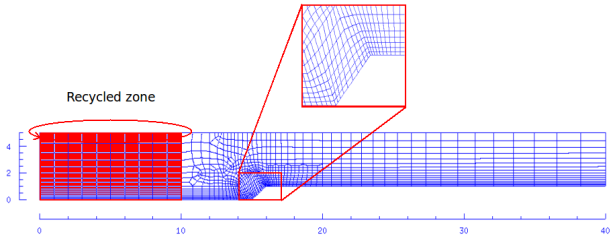

Figure 2: Two-dimensional FFR quadrilateral element mesh with recycling zone.

Results

Mean Flow and Reattachment Length

The averaged fields have been analyzed to identify the main flow features. The speed-up factors, ΔS, given by $[\Delta u(z)L]/[u_0(2L)H]$, uses the same calculation as that found in Bitsuamlak's review paper (Bitsuamlak et al., 2004) to compare our results to those in the literature. In these expressions H represents the height of the ramp, L represents the horizontal distance from the crest to where the ground elevation is half the height of the ramp, $\Delta u(z)$ represents increase in velocity, i.e., $u(z) - u_0(z)$ at height z above the local ramp surface, $u_0(2L)$ represent upstream reference velocity at the height $2L$ above the ground respectively, similarly $u_0(z)$ represent upstream reference velocity at height z above the ground respectively, Figure 3(a). Figure 3(b) compares our result with typical results used in Bitsuamlak's review paper (Bitsuamlak et al., 2004). The mean velocities accelerate on the edge due to surface elevation. For different geometries of escarpments ($H/L = 0.2$ to 1.2), normalized speed-up factors from literature and our results are fairly similar. Note that speed-up factors from previous studies tend to neutralize further away the surface. However our results show minor decline due to the blockage ratio of 0.2 downstream. Figure 3(c) represents normalized speed-up values normal to the edge at $1H$ downstream of the edge. By comparing four different yawed flows, we found that streamwise mean velocity of all cases have reverse flow regions, i.e. $\Delta S < 0$, indicating re-circulation zones. Velocity profiles at $y \geq 0.5$ are nearly identical for all yaw angles, indicating that the sweep-independence principle holds. Profiles for flow near the surface $y \leq 0.5$ begin to deviate, indicating that near-wall speed-up factor are influenced by the tangential wall frictions. We also found that flows without yaw angle give maximum speed-up ratio near the wall. A comparison of speed-up factors along inflow direction is done in Figure 3(d). Again, speed-up factors without yaw angle are the highest($\Delta S = 0.37$ at $z = 0.31$)). However the sweep-independence principle no longer holds here as ΔS decreases with increasing yaw angles.

The streamlines reported in Figure 4 represent the recirculation zones in different yawed flows. The flow is from left to right, with the display of streamwise velocity contours. It is well-known that the separation regions occur in front of and on the

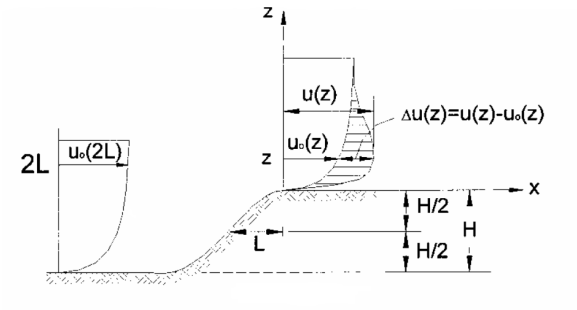

(a)

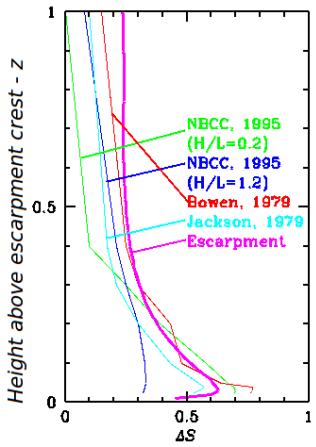

(b)

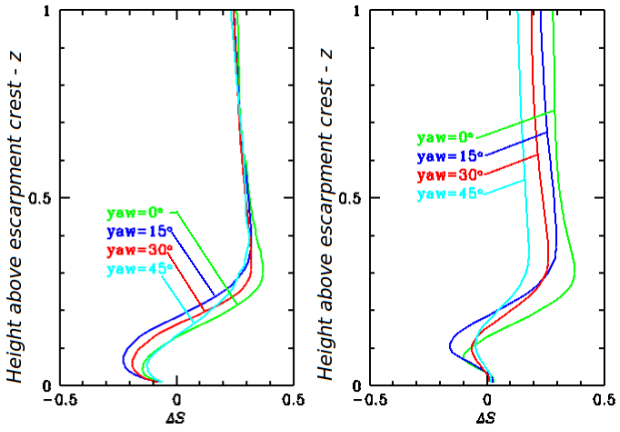

(c) (d)

Figure 3: (a) definitions of parameters for calculations of normalized speed-up ratio; (b) normalized speed-up ratio and typical results from literature (Bitsuamlak et al., 2004); (c) dimensionless velocity speed-up factors, normal to the edge (x), at $1H$ downstream with yaw angle 0°, 15°, 30° and 45°; (d) dimensionless velocity speed-up factors, along the inflow ($\hat{x}$), at $1H$ downstream with yaw angle 0°, 15°, 30° and 45°;

edge in the FFS flow. The present DNS obviously represent the same characteristic flow configuration as that found in the FFS flow. The upstream separation arises from the adverse pressure gradient caused by the blockage of flow at the ramp face. In this study separation points and reattachment points are almost fixed in each yawed flow. Therefore we focus on the second reattachment length as it is more difficult to predict. Table 2 represent the downstream reattachment length with two proposed coordinates at different yaw angles. The reattachment lengths normal

to the edge decreased slightly as the yaw angle increased from 0° to 45°. While in the coordinates aligned with the incoming flow, the reattachment lengths gradually increased with increasing yaw angle. In previous studies of rearward-facing step of swept flow (Fernholz et al., 1993; Kaltenbach and Janke, 1999), the invariance of x_R was interpreted in the sense that the sweep-independence principle holds for the flow over a swept step. There are few aspects which might be partially responsible for the observed differences between forward-facing step and backward-facing step flows: (i) compared to backward steps, which contain only one separation-reattachment region, forward step flow has more complex turbulence as they contain two separation-reattachment regions, (ii) fully developed turbulent upstream conditions is used in this study comparing to laminar upstream conditions in previous studies, which tends to introduce higher level of turbulence intensities, (iii) with $\delta/H \approx 5$, which is one of the parameters governing the size of the reverse flow region (Adams, 1984), is considerable larger than that in the previous studies where $0.03 \leqslant \delta/H \leqslant 0.12$, (iv) Reynolds number is different.

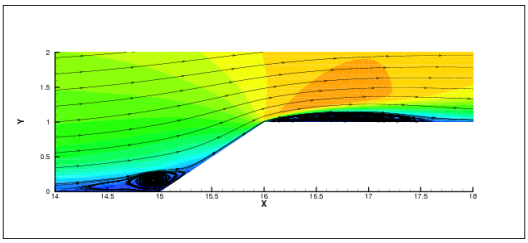

(a) $\alpha = 0°$

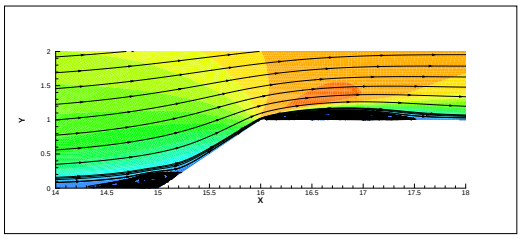

(b) $\alpha = 15°$

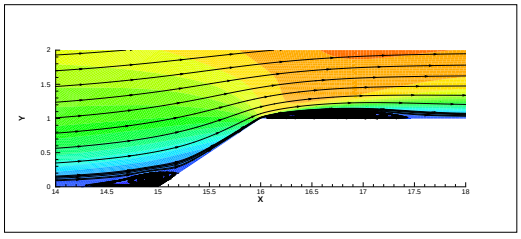

(c) $\alpha = 30°$

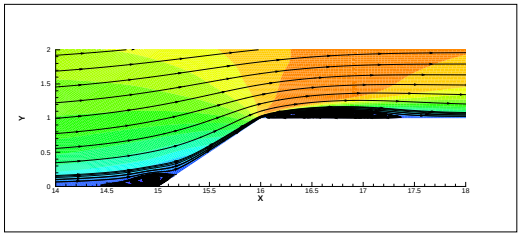

(d) $\alpha = 45°$

Figure 4: Streamlines around the ramp

Instantaneous Flow Field

The instantaneous velocity fields have been analyzed to educe turbulence coherent structures and study their dynamics. Jeong and Hussain (1995) suggests vortices are well-represented by connected regions where the second largest eigenvalue(λ_2) of the tensor $S_{ik}S_{kj} + \Omega_{ik}\Omega_{kj}$ is negative, here $S_{ij} \equiv (u_{i,j} + u_{j,i})/2$ and $\Omega \equiv (u_{i,j} - u_{j,i})/2$ are the symmetric and antisymmetric parts of the velocity gradient tensor $u_{i,j} \equiv \partial u_i/\partial x_j$. The top view of isosurfaces of $\lambda_2 = -50$ in $x-z$ plane at $y = 1.05H$ for various yaw angles reveals collections of vortices near-wall structure (Figure 5). Clearly, the dominant vortices are aligned predominantly with incoming flow ($\hat{x}$). Most of λ_2 regions occur around the ramp, which are known as the low-pressure regions. It is remarkable that yawed flow vortices become more intense than zero sweep. A possible cause for the observed increase in vortices in near wall region for high yaw angle is the fact that vortices which are not aligned with the homogeneous direction experience an extensional strain along their axis. Note that the $-\lambda_2$ tend to incline at a positive angle respect to the x-direction ($x-y$ plane, not shown). It is not clear to see some roller or rib structures. Though hairpin vortex line bundles do occur, the hair pin vortex are yet to confirm.

	downstream reattachment lengths	
yaw angle	R_x	$R_{\hat{x}}$
0°	$1.60H$	$1.60H$
15°	$1.53H$	$1.58H$
30°	$1.45H$	$1.67H$
45°	$1.35H$	$1.95H$

Table 2: Downstream reattachment length in two coordinates with various yaw angles.

The behavior of flow over a surface associated with separation usually results in a pattern of lines emanating from critical points where the shear stress, τ, are identically zero Perry and Chong (1994). In the two-dimensional or asymmetric cases, separation from the surface is identified at the point where shear stress reverses, and reattachment is where shear stress becomes positive again. Many investigations have dealt with a statistical description in terms of parameters like skin friction coefficient, mean separation length, reattachment point and turbulent intensities. With increasing computer power the geometric separation receives more and more attention as a time-dependent three-dimensional problem. Given the critical points interpretation in Perry's paper Perry and Chong (1994), streamline shown in Figure 6 are used to identify the flow patterns. The reverse streamlines gathered in a near vertical line, known as the collection of separation points. There are few streamlines from upstream that joins this line, which indicates the three-dimensional flow separation feature. Inside the recirculation region, there are number of critical points occur within the field of view. Among these critical points, node and saddle are most obvious. Surface bifurcation lines can also be visualized, which is an evidence of present of the longitudinal vortices. Note that all the critical points occurs at the zero u velocity.

Discussion

This study applies to the low Reynolds number range. Further investigation of greater Reynolds number is undertaken by spectral vanishing viscosity method(SVV).

Another segment of the project is carried out by Monash PhD candidate Jerome Rowcroft, whose research focus is on experimental investigation of wind flow over escarpments.

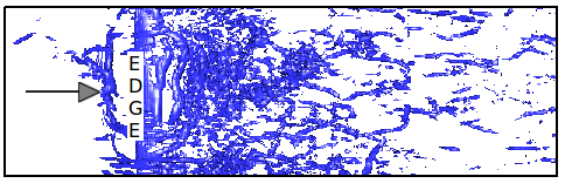

(a) $\alpha = 0^\circ$

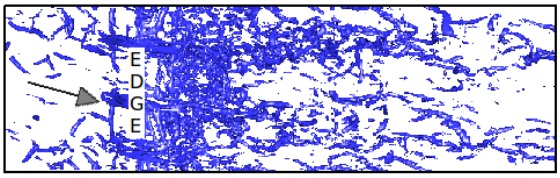

(b) $\alpha = 15^\circ$

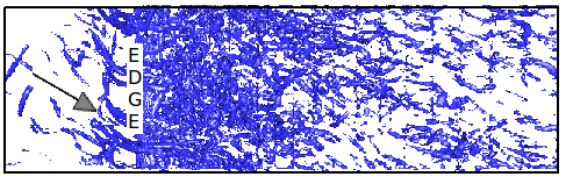

(c) $\alpha = 30^\circ$

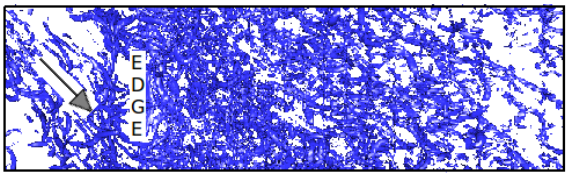

(d) $\alpha = 45^\circ$

Figure 5: Top view of the isosurfaces of $\lambda_2 = -50$ $x-z$ plane at $y = 1.05H$

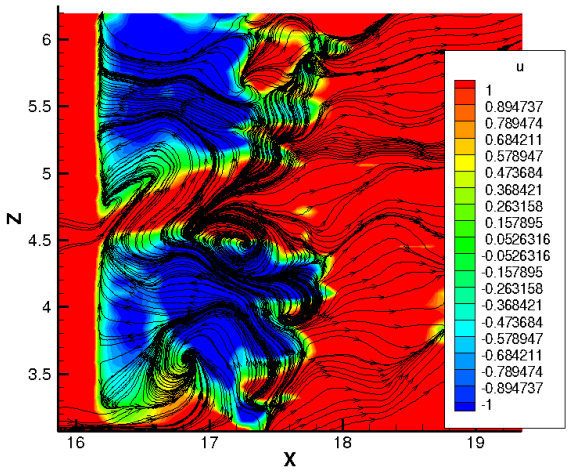

Figure 6: Contour of u velocity and streamlines of $x-z$ plane around the ramp, $yaw = 15^\circ$

Conclusions

We have investigated the yawed turbulent flow over a ramp at $Re_H = 2000$ with the emphasis on isolating influence of sweep. Shortening of the separation region along streamwise and an increase in inflow direction are found in the yawed flows.

The decomposition of the flow into ramp-normal components shows decrease trends if profiles of speed-up are compared at the same normalized position with increasing yaw angle. At a certain height above the ramp, the speed-up shows approximate collapse.

The λ_2-based coherent structures eduction scheme is generally applicable to this study. Observation of roller structure is found in the field. Hairpin vortex is believed to occur. An increase in vortices are found with increased yaw angle.

Acknowledgments

This research was supported by the ARC Industry Linkage project grant (LP100100746) between Monash University, Hydro Tasmania and Suzlon Energy.

References

Adams, E. W. (1984). *Experiments on the structure of turbulent reattaching flow*. PhD thesis, Stanford Univ., CA.

Bitsuamlak, G. T., Stathopoulos, T., & Bédard, C. (2004). Numerical evaluation of wind flow over complex terrain: Review. *Journal of Aerospace Engineering*, 17(4):135–145.

Bowen, A. & Lindley, D. (1977). A wind-tunnel investigation of the wind speed and turbulence characteristics close to the ground over various escarpment shapes. *Boundary-Layer Meteorology*, 12:259–271. 10.1007/BF00121466.

Cochard, S., Montlaur, A., Fletcher, D., Letchford, C., & Earl, T. (2012). Vortex formation above prismatic-shaped cliffs; an experimental and numerical investigation. In: *Proceedings of 15th Australasian Wind Engineering Society Workshop*, pages 888 – 894.

Fernholz, H., Janke, G., Kalter, M., & Schober, M. (1993). On the separated flow behind a swept backward-facing step. In: *Physics of Separated Flows: Numerical, Experimental and Theoretical Aspects*, volume 40, pages 200–207.

Jensen, N. (1983). Escarpment induced flow perturbations, a comparison of measurements and theory. *Journal of Wind Engineering and Industrial Aerodynamics*, 15(1-3):243 – 251.

Jeong, J. & Hussain, F. (1995). On the identification of a vortex. *Journal of Fluid Mechanics*, 285:69–94.

Kaltenbach, H. & Janke, G. (1999). Direct numerical simulation of flow over a swept rearward-facing step. In: *Direct and Large-Eddy Simulation III*, P. Voke, N. Sandham, & L. Kleiser, ed., volume 7 of *ERCOFTAC Series*, pages 393–404. Springer Netherlands.

Lund, T., Wu, X., & Squires, K. (1998). Generation of turbulent inflow data for spatially-developing boundary layer simulations. *J. Comput. Phys.*, 140:233–258.

Perry, A. & Chong, M. (1994). Topology of flow patterns in vortex motions and turbulence. *Applied Scientific Research*, 53:357–374. 10.1007/BF00849110.

Sherry, M., Lo Jacono, D., & Sheridan, J. (2010). An experimental investigation of the recirculation zone formed downstream of a forward facing step. *Journal of Wind Engineering and Industrial Aerodynamics*, 98(12):888 – 894.